Accepted for publication in *Engineering Structures*, May 2014

Debonding along the fixed anchor length of a ground anchorage

A.R. Akisanya[1] and A. Ivanović

School of Engineering,
University of Aberdeen,
Aberdeen AB24 3UE, U.K.

Abstract

Ground anchorages are the main means of support used for safety aspects in mining and tunnelling industry. Poor installation of ground anchorages can result in partial debonding between the tendon and the grout. The effects of debonding on the load carrying capacity of a model anchorage are examined by pull out tests. The load carrying capacity is found to decrease with increasing length of pre-existing debonding at the tendon-grout interface. The fracture toughness of the tendon-grout and of the ground-grout interfaces is measured over a wide range of mixed-mode loading and the results are used to assess the likelihood of debonding at the interfaces in a ground anchorage system.

Keywords: Anchorages; Pull-out tests; Debonding; Interface fracture; Fracture toughness.

1. Introduction

Ground anchorages are safety critical elements for supporting structures like tunnels, mines and retaining walls. There are numerous ways of classifying anchorages: active or passive, depending on whether they are pre-stressed or used as reinforcement; and single or multi-strand, depending on whether the tendon is a bolt or a cluster of strands. This paper considers a single, active rock anchor system.

[1] Corresponding Author. Email: a.r.akisanya@abdn.ac.uk. Fax: +44 1224 272497

The main components of an anchorage system are the tendon, an anchor head assembly (bearing plate and a nut), and the grout [1] (see Fig. 1). The grout is made of resin (usually polyester based) or a cement mixture, while for a rock bolt, the tendon is usually made of steel.

Rock bolts are bonded to the surrounding rock mass along the fixed length (Fig 1) and, if active, are tensioned. The role of the bond is to transfer the load from the tendon (e.g. steel bar or bolt) to the surrounding rock mass or ground. Thereafter, the terms rock and ground are used interchangeably to denote the surrounding material that is bonded to the tendon through the grout. The unbounded length the tendon is classified as free length (if within the ground) and protruding length (outside the ground), see Fig. 1. A pre-tensioned tendon induces a compressive stress in the surrounding rock mass which consequently inhibits cracking of the rock and thus enhances the stability [2]. Differential movement of the rock mass can also induce compressive stress in the surrounding rock.

During installation of an anchorage or in service, cracks may initiate and grow within the anchorage system leading to loss of load carrying capacity [2]. The cracks may initiate within the grout, at the tendon/grout interface or rock/grout interface, while the tendon may fail during installation especially in passive anchorages. Further, ingress of ground water may lead to corrosion of the tendon resulting in the development of tendon/grout interface crack [2]. The actual location of failure in a particular application depends on the mechanical and fracture properties of the materials, the characteristics of the interfaces, and the compatibility of the grout with the bolt and surrounding rock. For a steel tendon, the strength and toughness of the steel are much greater than the corresponding parameters for the grout, surrounding rock and the interfaces. It is not surprising therefore that most observed failures of anchorages in practice occur at one of the two interfaces: rock/grout and tendon/grout interfaces [3, 4, 5]. Thus, the strength and toughness of these interfaces play a major role in determining whether an anchorage can withstand the load they are designed to hold. It is therefore important to understand the role and characteristics of the interfaces since they influence significantly the overall performance of the anchor system. Surprisingly,

the quantification of the interface toughness and the relationship of the toughness to failure mode and location has received little attention in the literature on ground anchorages.

Currently, the assessment of the load carrying capacity of ground anchorages is based on analysis of the induced stresses in a "perfect" anchorage (i.e. no defects). Consider an anchorage consisting of a tendon (e.g. steel bolt) and grout with Young's modulus E_s and E_c, respectively, and bolt and borehole diameter d_s and d_h, respectively. Let the Young's modulus of the surrounding rock mass or ground be E_g. When the tendon, which is assumed to be perfectly bonded to the grout along the fixed anchor length, is subject to a uniaxial tensile stress P, the induced interfacial stresses along the fixed anchor length are function of E_c/E_g and the relative diameter of the tendon to that of the borehole, d_s/d_h.

Linear elastic finite element analysis of a cylindrical anchorage with 'perfect' bonding shows that the shear stress at the ground/grout interface decreases in magnitude from the proximal end to the distal end of the anchor, while the magnitude of the maximum shear stress increases with decreasing value of E_c/E_g [6], see Figure 2. For ground anchorages installed in hard rocks, E_c/E_g ranges between 0.1 and 1, which according to Figure 2, produce a power-law distribution of shear stress along the fixed length. (Recall that E_c is the Young's modulus of the grout while E_g is the Young's modulus of the ground or rock mass.) However, design standard for ground anchorages, e.g. BS8081 [2], is based on a uniform shear stress distribution. For soft rocks ($E_c/E_g \geq 10$), the load distribution is more uniform. As the maximum shear stress occurs at the proximal end where the ground/grout interface intersects the free length section, interfacial debonding or crack is therefore more likely to initiate from that end.

The interfacial stresses in addition to being governed by elastic properties of the materials, are also influenced by the geometry of the borehole and tendon. For a given size of the tendon, the shear stress at the ground/grout interface becomes more uniform along the interface and the magnitude of the stress decreases with decreasing diameter of the borehole resulting in increased load capacity of the anchor system as the borehole diameter is reduced [7-9]. Thus, for a given bolt

size and grout type, the load capacity of the anchorage increases with decreasing borehole diameter (or decreasing radial thickness of the grout). This is consistent with the fracture response of adhesively bonded sandwiched joints where it has been shown for plane strain geometry subject to remote tension that the fracture stress increases with decreasing thickness of the adhesive layer [10, 11]. Thus, a higher bond strength and anchorage load capacity can be achieved with a reduced annulus of a perfectly bonded anchor system. However, this has implications for the installation of anchorages as it limits the volume of grout available for bonding which could lead to the development of unbounded patches during installation. Consequently, there have been few experimental studies to examine the effects of dimensions and material properties on the load capacity of anchorages.

For example, Ivanovic and Neilson [12] carried out experiments using scaled laboratory model of anchor systems consisting of a concrete to simulate the ground, an epoxy resin grout and steel rebar; E_c/E_g = 0.3 and E_c/E_s = 0.06. The rebar had a diameter of d_s = 22 mm and the borehole had a diameter of d_h = 30 mm. The applied axial load for perfectly bonded rebar increases almost linearly with increasing axial displacement until failure occurred at the concrete/grout interface; the failure load increases with increasing fixed anchor length. There was a drop in load following the initiation of the debonding, and subsequently the sliding of the rebar occurred at almost a constant load. However, in a separate study by Benmokrane et al. [5] where cement grout was used (E_c/E_g = 1 and E_c/E_s = 0.2), and the diameter of the steel bar and borehole was 15.8 mm and 38 mm respectively, failure occurred at the tendon/grout interface. The difference in the location of the interface failure was believed to be due to the difference in the thickness of the annulus used in the two studies as well as the difference in materials used for grouting; but this was not verified.

The initiation and growth of debonding at the tendon/grout and ground/grout interface involves frictional sliding. Hence the load capacity of ground anchorages is influenced by the level of normal pressure on the interface. The effect of normal pressure on load capacity of anchorages is usually assessed either by applying a uniform constant confining pressure to a model anchorage or by using an outer shell with a relatively high stiffness to represent the surrounding rock mass [13-16].

In the latter, which is closer to what happens in the field, the magnitude of the radial confining pressure increases as the applied load increases due to the resistance to lateral deformation provided by the stiffness of the surrounding rock mass. The load capacity of an anchorage increases with applied normal interface pressure up to a certain magnitude of pressure above which there is no significant enhancement to the load capacity [14-16]. Soft rocks with low radial stiffness will not generate a high enough radial pressure and this can lead to the development of radial cracks, while hard rocks can generate relatively high radial pressure which supresses the development of radial cracks and thus significantly enhances the load capacity of the anchorage [17].

Majority of the earlier work on the stress distribution and load capacity of anchorages focused on 'perfect' bonds. A good quality bond along the fixed anchor length is essential for effective performance of any anchorage system. Although, field data and laboratory experiments suggest majority of anchorages fail by debonding at one of the interfaces [3, 5], it is not clear whether this is due to a debond created during installation or initiated post installation. It is generally believed that microcracks are initiated at the proximal end during pre-tensioning of anchorages; this is recognised in the design standard [2] through a recommended increase in the design free anchor length by an estimated length of the debonding. However, there is no experimental validation of the relationship between the level of the pre-tension and the length of induced microcracks, or of the role of debonding in the load capacity of anchorages.

The load-displacement response and the failure characteristics of a rock anchor system may, to some extent, be likened to those for fibre pull out in fibre-reinforced composites. Fibre pull out from the matrix of fibre-reinforced composites has been studied extensively in the literature using shear lag method, energy based method, fracture mechanics approach, and the cohesive zone model, see for example Refs. [18-23]. The fracture mechanics approach views the pull out as a mode II interface crack (i.e. sliding mode). Friction effects associated with sliding are important in systems with a residual compressive stress across the fibre/matrix interface [19, 20], in the same way as the confining pressure affects the load capacity of anchorages. However, unlike the pull out of a fibre from the matrix of fibre-

reinforced composites where there is only one controlling interface (i.e. fibre/matrix interface), rock anchor systems have an interlayer between the bolt and the surrounding rock and therefore there are two interfaces, either of which could be a site for initiation of debonding. In addition, the steel bars in rock anchors are larger in size (order of tens of millimetres compared with micrometres for fibres) and usually rebar with profiled surface which introduces additional complexity of mechanical interlock. Furthermore, the initial growth of the debonding from the proximal end of a rock anchor can be dominated by mode I deformation (i.e opening mode) [21].

The effect of the interaction between an electrical field and mechanical loading on debonding during fibre pull-out or push-out using the energy based method is considered by Wang and Qin [24]. The current paper focuses only on mechanical loading and uses fracture mechanics concepts to examine the effects of the fracture toughness of the rock/grout and tendon/grout interface on the location and mechanism of failure. Experiments on laboratory-scale model of a steel bar-grout-concrete anchorage system, with and without pre-existing debonding, are used to assess the effect of pre-existing debonding on the load capacity of the anchor. The effects of the surface characteristics of the bolt are examined by considering a smooth surfaced bar and a rebar. Further fracture experiments are carried out to quantify the fracture toughness of the concrete/grout and steel/grout interfaces over a wide range of loading. The fracture toughness results are used to assess the likelihood of crack initiation and growth at one of the interfaces in a ground anchorage rather than the other.

2. Tendon pull out in an anchorage system

2.1 *Materials and experimental methods*

Experimental study was undertaken to investigate the role of pre-existing debonding on the load capacity of an anchorage. The experimental set-up and concepts are similar to those adopted in [12]. Concrete is used to model the surrounding rock or ground while a polyester two-part slow-setting epoxy resin[2]

[2] Lockset(R) Resin Capsule, manufactured and supplied by Minova International Limited, Oxon, U.K..

was used as the grout. Two types of tendon were considered: a steel bar with a smooth surface and a rebar; the latter is commonly used in practice.

As mentioned above, the response of an anchorage system depends on the relative stiffness of the constituent materials. The Young's modulus of each of the materials was determined. Tensile test was carried out on the steel material using a solid circular cylinder with a 5 mm diameter and 25 mm gauge length in accordance with ASTM E8M [25]; the axial and transverse strains were measured using strain gauges. Similar tensile test was carried out on the epoxy resin. In this case, dumbbell shaped specimens were prepared to ASTM D638 [26] using a specially made mould to cast the specimens. The specimens were left to cure at room temperature for 24 hours before testing at a nominal strain rate of 2.5×10^{-4} s^{-1}. The properties of the concrete were determined using a 100 mm cube subjected to uniaxial compression; the concrete was cured for 28 days before testing. In all cases, three nominally identical specimens were tested; the stress-strain responses were identical to within a few percent. The average measured properties are summarised in Table 1. Using the measured properties, the ratio of the Young's modulus of the resin grout to that of the concrete, $E_c/E_g = 0.23$.

A schematic diagram of the model anchorage system is shown in Figure 3a. Concrete cylinders of 200 mm in diameter and 400 mm in length containing a 30 mm diameter borehole were used. A PVC mould with 5 mm wall thickness and 200 mm internal diameter was used to cast the concrete. In order to prevent the formation of surface cracks, the borehole was not created by drilling the concrete. Instead, the borehole was cast in-situ using a plastic tube which has an outer diameter equal to the borehole diameter (d_h = 30 mm), and with one of the two ends sealed. The surface of the tube was lubricated with a mould release agent. The tube was then suspended at the centre of the PVC mould with the aid of a jubilee clip and a wooden plank ensuring the sealed end was inside the mould (see Figure 4). The plank, with the tube attached, rested on top of the PVC mould while the concrete was poured into the mould to the required height of 400 mm. The tube was gently given a few complete rotations every hour as the concrete sets, and was subsequently slowly pulled out by hand after about 7 hours while the concrete was left for 28 days to fully cure. Although the borehole is normally drilled in

practice resulting in a non-smooth borehole surface, the process of casting the borehole in-situ leaves a relatively smooth borehole surface and eliminates the development of surface cracks associated with drilling. This allows an assessment of the failure mechanism in relation to the measured fracture toughness.

The ratio of the Young's modulus of the resin grout to that of the concrete used in this study, E_c/E_g = 0.23 which is well within the range $0.1 \leq E_c / E_g \leq 1$ for hard rocks. We note that the test set-up is consistent with a constant stiffness test as no external confining pressure was applied. However, the combined effect of using a relatively large external diameter of the concrete d_g (= 6.7d_h) where d_h is the borehole diameter and low ratio of E_c/E_g (= 0.23) and leaving the PVC cylindrical mould in place while testing provide a high constant radial stiffness leading to in-situ development of high confining pressure during testing. This we believe will limit or eliminate the development of radial cracks.

The diameter of the steel bar used was d_s = 20 mm and the bonded length of the bar was 210 mm. The borehole was cleaned using compressed air to remove any debris after which a predetermined volume of the two-part resin was put inside the borehole and thoroughly mixed.

The surface of the steel bar was cleaned using acetone and inserted in the borehole containing the resin using a specially made guard, similar to that used for the in-situ casting of the borehole, to ensure the bar was centrally positioned in borehole. Two cases were considered: (i) no initial debonding at any of the interfaces and (ii) a pre-existing debonding at the steel/grout interface. In order to simulate the debonding, the surface of the steel bar was covered with an electrical tape from the free end up to the desired length and the surface of the tape was sprayed with a mould release agent prior to inserting the bar in the borehole containing the resin. The tape prevented the bonding of the steel bar to the resin in the region where the tape was placed at the proximal end. The debond length, *a,* considered were: $a = 0$, $a = d_s$ and $a = 2.5d_s$ where d_s (= 2 cm) is the diameter of the steel bar. The model anchorage was left to cure at ambient temperature for 24 hours before testing. As the specimen preparation and testing were carried out at ambient temperature, there was no misfit strain due to thermal expansion

mismatch and thus residual stresses across the steel/grout and concrete/grout interfaces would be minimal.

In order to ensure the concrete was axially constrained during the pull out test, a specially constructed steel frame was used, see Fig. 3, while the PVC mould provided radial constraint to the deformation. The frame consisted of a steel plate at the base and another plate at the top of the model anchorage. The plates were connected by bolts and nuts as shown in Figure 3. The assembled anchorage is mounted on a servo-hydraulic testing machine, see Figure 3b. Pull out tests were performed in displacement control at crosshead speed of 5 mm/min. The applied load and the displacement, which was measured using a LVDT (Linear Variable Differential Transformer), were continuously recorded using a computerised data logger.

For the model anchorage with smooth steel bar, two nominally identical anchorages were tested for each of debond length $a = d_s$ and $a = 2.5d_s$ where d_s (= 2 cm) is the diameter of the steel bar, while one model anchorage was tested for each of the other cases considered. The results of the replicated tests were used to confirm the consistency of the test method and data.

2.2 *Pull out test results and discussion*

Typical load versus displacement response of the model anchorage is shown in Figure 5. The presence of an initial debonding at the grout/steel bar interface has a significant effect on the load-displacement response. With no initial debond, the load for the smooth steel bar increases, almost in a linear manner, with increasing displacement until the maximum load at which failure occurred. The failure, by debonding at the concrete/grout interface, is accompanied by a sudden drop in the load; this is an indication of an unstable crack growth. Subsequently, sliding occurred at almost a constant load of about 22 kN (Fig. 5a). For smooth bars with pre-existing debonding, there was no noticeable drop in load following the initiation of crack growth; the initiation of debonding and subsequent sliding of the bar occurred in a stable manner and at a constant load. The load for stable sliding

was found to slightly increase with decreasing size of the initial debonding. The results for the smooth bar without initial debonding are consistent with other published results for similar anchorages [12].

We observed a similar trend in the load-displacement response for the tests undertaken on a rebar (Fig. 5b). However, the maximum load for the case without initial debonding and the constant load for stable sliding for a rebar are greater than the corresponding value for a smooth bar due to shear mechanical interlock associated with the rebar [2]. For the model anchorage without pre-existing debonding, we note that the peak load of 84 kN for the rebar and 52 kN for the smooth bar are lower than the typical failure load in practice. It is well known that the peak load increases linearly with the fixed anchor length [2]. In the current study the fixed anchor length was 0.21 m while in practice the fixed anchor length ranges between 2 m and 10 m depending on the type of rock formation. Thus, the results obtained in the present study are therefore consistent with the fixed anchor length used in the model anchorage. Furthermore, the measured failure load for the model anchorage without pre-existing debonding and with a rebar is consistent with the reported value of 70 kN by Bermokrane et al. [5] for a model anchorage with a cement grout and similar relative geometric parameters as considered in the current study. For a drilled borehole where the concrete/grout interface has a higher shear strength than for the steel/grout interface, failure is more likely to occur at the steel/grout interface and at a much higher load than obtained in the present study [14-16].

It is obvious from Fig. 5 that the existence of initial debonding results in reduction of the load capacity of the anchorage; the maximum load decreases with increasing debond length, see Fig. 6. The maximum load capacity for debond length of $2.5d_s$, where d_s (= 2 cm) is the steel bar diameter, is almost half that without any debonding (Figure 6). Here the load capacity is defined as the load required for the initiation of interface crack growth. It could be argued that the reduced load capacity for cases with pre-existing debonding at the proximal end is associated primarily with the reduction in the fixed anchor length. This would be the case if failure occurred at the grout/steel interface which is not the case in the current study (see Figure 7). The failure load is directly proportional to the fixed

anchor length [2]. For the rebar without pre-existing debonding, the bonded length of the steel bar was 0.21 m and the failure load was 84 kN. With pre-existing debond length of $2.5d_s$ (= 0.05 m), the bonded length of the steel bar reduced by 23% while the failure load was reduced by almost 50% relative to that without pre-existing debonding. The presence of the pre-existing debonding is therefore a major factor in the measured reduction in load capacity of the model anchorage. The present results reinforce the need to consider the presence of debonding in determining the load capacity of an anchorage. It is important to note that once debonding initiates at the maximum load, the debonding occurs along the whole of the fixed anchor length leading to large scale sliding of the bar from the anchorage.

Despite the pre-existing debonding at the steel/grout interface, we note, surprisingly, that failure occurred at the concrete/grout interface in all the cases considered; the grout remained bonded to the bar while it slid out of the concrete, see Fig 7. Visual examination of the tested model anchorage revealed no radial cracks (Figure 7). This suggests the diameter of the concrete relative to the diameter of the borehole is sufficiently large and the stiffness of the PVC mould is sufficiently high to provide the radial confinement necessary to prevent the initiation of radial cracks.

We expected failure to initiate from the pre-existing debond crack as the singularity at the tip of the steel/grout debond crack is stronger than that at the interface corner between the concrete and grout. There is a competing mechanism of crack initiation and growth at the two interfaces, with the chosen location of crack growth being the interface with the lower fracture toughness (or resistance) at the applied load. The pull-out test results suggest the steel/grout interface is much tougher than the concrete/grout interface considered in this study. We postulate that in addition to the interface crack that was intentionally introduced at the steel/grout interface, the mould release agent used for the in-situ casting of the borehole may have reduced the concrete/grout interface toughness and small microcracks may have been developed at the proximal end of the concrete/grout interface during the construction/curing of concrete and assembly of the small scale anchorage model. In order to assess whether a pre-existing crack or defect at the concrete/grout interface will propagate in preference to a crack at the steel/grout bar interface a

more detailed analysis of the crack driving force and the fracture toughness of the interfaces is needed. In the following, interface fracture mechanics concepts and further experimental results on the fracture toughness of the two interfaces are used to justify the choice of fracture location observed in the model anchorage.

3 Application of fracture mechanics to debonding in ground anchorage

The experimental results of the pull-out test presented above showed the detrimental effect of pre-existing interface cracks on the load capacity of an anchorage. Interface fracture mechanics concepts, which have been successfully applied to the prediction of failure in layered solids and adhesive joints [27 - 29], are used here to explain the observed debonding at the concrete/grout interface rather than at the steel/grout interface in the pull-out test described above. For completeness, a summary of the relevant interface fracture mechanics concepts are presented; and this is followed by measurement of the fracture toughness of the two interfaces.

3.1 *Overview of interface fracture mechanics*

Consider a sandwiched joint containing a thin linear elastic interlayer of thickness *h* (referred to as material 2) sandwiched between two identical linear elastic solids (referred to as material 1). Both materials are isotropic and homogeneous, with Young's modulus E_j and Poisson's ratio ν_j, where *j* (= 1, 2) denotes the material number. We assume a crack exists at one of the interfaces between the interlayer and the adhrend material 1, and the joint is subject to a remote stress σ^∞ normal to the crack surface and a remote in-plane shear stress τ^∞.

In the absence of an interlayer or with an interlayer whose elastic properties are identical to those of the adherends, the crack tip stress field is characterised by the Mode I (opening) and Mode II (sliding) stress intensity factors. The relative mode I to mode II is quantified by the phase angle of the remote loading, given by

$$\phi = \tan^{-1}\left(\frac{\tau^\infty}{\sigma^\infty}\right) = \tan^{-1}\left(\frac{K_{II}}{K_I}\right) \qquad (1)$$

ϕ = 0 implies pure mode I (opening) and ϕ = 90^o implies pure mode II (sliding). Ground anchorages are loaded remotely in pure mode II. Without the interlayer, the mode-mixity associated with the remotely applied load is identical to the mode-mixity of the stress state near the crack tip characterised by the stress intensity factors, K_I and K_{II}, see eqn. (1).

For an interlayer whose elastic properties are different from those of the adherends, the mode mix ahead of the interface crack in a sandwiched joint is different from that of the remotely applied loads. When a sandwiched joint containing an interface crack is subject to a combination of remote tensile stress σ^∞ and shear stress τ^∞, the singular stresses directly ahead of the crack are given by [30]

$$\sigma_{yy} + i\sigma_{xy} = (K_1 + iK_2) r^{-\frac{1}{2}+i\varepsilon} \qquad (2)$$

where $i = \sqrt{-1}$, (*x, y*) and (*r, θ*) are respectively the Rectangular Cartesian and cylindrical polar coordinates centred at the crack tip, $K = K_1 + iK_2$ is the complex stress intensity factor for the interface crack, and ε is a constant function of the elastic properties of the materials [27-29]. For the materials properties of the model anchorage system given in Table 1, ε = -0.08 and -0.09 for steel/grout/steel and concrete/grout/concrete sandwiched joint respectively.

If the material constant $\varepsilon \neq 0$, the interfacial stresses given in eqn. (2) are oscillatory as the crack tip is approached. This complicates the definition of the local interfacial mode mix (i.e. ratio of shear stress to normal stress) near the crack tip. The generally adopted approach, suggested by Rice [30] is to define the mode-mixity at a given distance from the crack tip. The distance is normally taken as the characteristic length scale of the geometry, which in this case is the thickness *h* of the interlayer. Thus the interface mode-mixity is measured by the phase angle

$$\psi = \tan^{-1}\left(\frac{\sigma_{xy}}{\sigma_{yy}}\right)_{r=h} = \frac{\mathrm{Im}\, Kh^{i\varepsilon}}{\mathrm{Re}\, Kh^{i\varepsilon}} \qquad (3)$$

The phase angle ψ for the interface crack is related to the phase angle ϕ of the remote loading according to [27]

$$\psi = \phi + \omega \tag{4}$$

where ω measures the effect of the mismatch in the elastic properties of the bonded materials on the interface phase angle. The values of ω are tabulated in [27]; ω = -13^o and -10^o for the steel/grout/steel and concrete/grout/concrete joint respectively. The stress intensity factor for the interface crack, $K = K_1 + iK_2$, scales linearly with the magnitude of the remotely applied loads and depends on the details of the joint geometry and crack length.

The crack driving force for the interface crack is the interface strain energy release rate, G_i, given for plane strain deformation by [27]

$$G_i(\psi) = \frac{1}{2}\left[\frac{1-\nu_1^2}{E_1} + \frac{1-\nu_2^2}{E_2}\right] K\overline{K} \tag{5}$$

$\overline{K}$ is the complex conjugate of the interface stress intensity factor. Thus G_i is a function of the applied load and the geometry. As the magnitude of remotely applied load on the sandwiched joint increases, the magnitude of both the interface stress intensity factors and the interface strain energy release rate G_i increases. Crack growth starts when the magnitude of G_i equals the interface fracture toughness Γ_I.

Unlike the toughness for monolithic brittle solids which is just a function of the material, the interface fracture toughness Γ_I is a function of the quality of the bond between the materials and also of the imposed loading measured by the phase angle ψ. The resistance to crack growth along an interface increases as the magnitude of the shear stress at the interface increases, i.e. $\Gamma_I(\psi)$ increases as $\psi \to \pm 90^o$ [28, 29]. Thus, the interface between two materials does not have just one value of fracture toughness; the toughness depends on the mode mixity of the

interface stress state. The maximum load carrying capacity for bonded joints would be obtained when the geometry is loaded predominantly in shear as it is the case in ground anchorages.

The onset of interface crack growth for a given mode mixity ψ is thus determined by the criterion

$$\frac{G_i(\psi)}{\Gamma_I(\psi)} \geq 1 \qquad (6)$$

where the interface fracture toughness Γ_I must be determined experimentally while the interface crack driving force G_i is normally determined numerically or analytically for the loading phase angle relevant to the application under consideration. For the ground anchorage, the phase angle depends on the relative elastic properties of the material, the relative geometric dimensions of the configuration, and crack length. For a given anchorage system, $\psi = \psi(F, a)$ where F is the applied pull-out force and a is the size of the pre-existing debond. Thus, for a given debond length a, eqn. (6) can be used to determine the failure load provided the solution to the crack driving force G_i and interface fracture toughness Γ_I are known. Note that G_i scales linearly with the magnitude of the remotely applied loads.

For a given rock bolt where a short crack exists at each of the two interfaces, failure would occur at the interface where relation (6) is first satisfied as the remote load is monotonically increased. Therefore, the assessment of the likely location of failure in a ground anchorage requires knowledge of the dependence of G_i and Γ_I on the phase angle ψ. In the following, we present the experimentally determined interface fracture toughness Γ_I for the steel/grout and concrete/grout interfaces and show why failure at the concrete/grout would preferentially occur for these material combinations.

3.2 *Experimental method for determination of interface fracture resistance*

Although ground anchorages are remotely loaded in pure shear ($\phi = 90^o$), we have measured the interface fracture resistance over a loading phase angle in the range $0 \le \phi \le 90^o$ for the steel/grout and concrete/grout.

Different specimen configurations can be used to measure interface fracture resistance, for example double cantilever beam, four-point bend, Brazil disc, etc. Many of the specimen geometries are only suitable for a narrow band of loading phase angle. We have chosen the Brazil disc specimen geometry for the current study as it is suitable for the application of loading over the range $0 \le \phi \le 90^o$. The use of this specimen geometry for measuring interface fracture resistance is well documented; see for example [28, 29].

Brazil disc specimens, with a configuration similar to that shown in Figure 8, were manufactured from semi-circular discs of steel and concrete. The radius R = 90 mm for the steel/grout and R = 50 mm for the concrete/grout; the out-of-plane thickness was t = 10 mm and the relative size of the starter crack was a/R = 0.2 in all cases. The grout used was from the same batch as that used for the pull out tests described earlier.

The bonding surfaces were thoroughly cleaned prior to bonding; compressed air was used for the cleaning of the concrete and an abrasive paper and acetone were used for the steel. A 0.02 mm thick aluminium foil coated with a silicone-based mould release agent was used to simulate the crack. The grout was placed between the two halves of the steel or concrete, and a slight pressure was applied to ensure bonding and control the grout thickness; the measured average thickness of the grout was 1.5 mm. The specimens were allowed to cure at ambient temperature for 24 hours before testing.

Diametrical compression tests were carried out in displacement control at a crosshead speed of 0.5 mm/min. A diametrical load P per unit out-of-plane thickness was applied at an orientation φ from the crack plane; φ controls the mode mix ϕ of the remote loading. A pure mode I remote loading (ϕ = 0) is obtained when φ = 0, and φ = 29° for pure mode II remote loading ($\phi = 90^o$) when a/R = 0.2. The

stress intensity factor solution for a Brazil disc fracture specimen is available in [31]. For a given failure load $P = P_f$, the stress intensity factors were determined as detailed in [31]; these were then used in eqn. (5) to calculate the interface fracture toughness Γ_i corresponding to the particular phase angle ϕ, as detailed in [28, 29].

3.3 *Fracture toughness of steel/grout and concrete/grout interfaces*

The interface fracture toughness is shown in Figure 9 as a function of both the remote loading phase angle ϕ and the interface phase angle ψ. As expected, the interface fracture resistance increases with increasing magnitude of the interface phase angle, with the maximum toughness occurring for pure remote shear (ψ = 77^o for steel/grout and ψ = 80^o for concrete/grout). We note that the fracture toughness for the steel/grout interface when $\psi = 77^o$ is about three times greater than for when $\psi = -13^o$, while for the concrete/grout interface the fracture toughness at $\psi = 80^o$ is almost ten times greater than when $\psi = -10^o$. Numerical studies of fibre pull-out in composite materials show that crack growth for shorter initial interface debonding (less than the fibre diameter) is dominated by the mode I while growth of longer initial interface debonding is dominated by the mode II. For the material combination and anchorage system considered in the current investigation, $\psi \to 80^o$ as the mode II component of the interface stress field near the crack tip increases.

More importantly is the significant difference in the magnitude of the fracture toughness for the steel/grout and concrete/grout interface; the former is significantly greater at the same loading phase angle. For pure mode II remote loading, which is most relevant to ground anchorages, the toughness of the steel/grout interface is nearly 2.5 times greater than that for the concrete/grout interface. This explains why failure occurred at the concrete/grout interface in the present study rather than at the steel/grout interface in the pull-out tests described earlier; concrete has been used in this study as a model material for rock or soil formation where anchorages are usually deployed. Although a drilled borehole will have a rougher surface and higher concrete/grout toughness than for the smooth

borehole surface was used in the model anchorage, the quantitative concrete/grout and steel/grout interface toughness presented in this paper will be useful in assessing the likelihood of failure at the two interfaces in a ground achorage.

4 Conclusions

The effect of debonding which may develop in ground anchorages during installation or in service on the load carrying capacity was studied by pull out experiments. The rock or ground was modelled using concrete and the grout was an epoxy resin. Both smooth bar and rebar were considered. The load carrying capacity was shown to decrease with increasing length of pre-existing debond length at the steel/grout interface, and the failure load for the rebar was greater than for the smooth bar due to mechanical interlock. Despite the presence of initial debond length at the steel/grout interface, crack growth and sliding occurred at the concrete/grout interface. To the authors knowledge, there is no reported work in the literature providing a quantitative assessment of the effect of pre-existing debonding on the load capacity of ground anchorages. The results presented in this paper when used in conjunction with conditioning monitoring of ground anchorages can provide useful insight into the integrity of ground anchors.

The fracture toughness of the concrete/grout and steel/grout interfaces was measured using the Brazil disc specimen over a wide range of loading phase angle. The concrete/grout interface was quantitatively shown to have significantly lower fracture resistance than the steel/grout interface leading to the occurrence of failure at the concrete/grout by debonding in the model ground anchorage system. The results presented in this paper show that it is possible in a ground anchorage system with a relatively smooth borehole surface to have pull out from the ground/grout interface even when a crack exists at the bolt/grout interface. Therefore, this study shows how the interaction between the toughness of the tendon/grout and rock-mass/grout interface influences crack development and consequent reduction in load capacity which is vital when monitoring the integrity of rock bolts.

Acknowledgement

The authors would like to thank Mr Mark Gourlay, Mr Douglas Craighead, Mrs Vita Mikucka and Miss Natalia Crespo for experimental assistance.

References

1. Ivanović A, Neilson RD, Rodger AA. Influence of prestress on the dynamic response of ground anchorages, *ASCE J Geotech Geoenv Eng*, 2002; 128: 237-249.
2. BS 8081:1989. British Standard Code of Practice for Ground Anchorages.
3. Durham RK. Anchorage tests on strain gauged resin bonded bolts. *Tunnels and Tunneling*, 1976; 73-76.
4. Yap LP, Rodger AA. A study of the behaviour of vertical rock anchors using the finite element method. *Int J Rock Mech Min Sci*, 1984; 21:47–61.
5. Benmokrane B, Chennouf A and Mitri HS. Laboratory evaluation of cement based grouts and grouted rock anchors. *Int J Rock Mech Mining Sci & Geomech Abstr*, 1995; 32: 633-642.
6. Coates DF and Yu YS. Three dimensional stress distribution around a cylindrical hole and anchor. *Proc. 2nd Conf Inst Soc Rock Mech*, 1970; 2: 175-185.
7. Yazici S and Kaiser PK. Bond strength of grouted cable bolts. *Int J Rock Mech Mining Sci & Geomech Abstr*, 1992; 29: 279-293.
8. Bažant ZP and Sener S. Size effect in pull out tests. *ACI Mater J*, 1988; 85: 347-351.
9. Hagan P C and Weckert S. *Anchorage and failure mechanisms of fully encapsulated rock bolts – Stage 2*, UNSW Mining Research Centre, ACARP Project C10022, 2002.
10. Akisanya AR and Meng CS. Initiation of fracture at the interface corner of bi-material joints. *J Mech Phys. Solids*, 2003; 51: 27-46.
11. Suzuki Y. Adhesive tensile strength of scarf and butt joints of steel plates. *Int J JSME Ser A*, 1987; 30: 1042-1051.
12. Ivanović A and Neilson RD. Modelling of debonding along the fixed anchor length. *Int J Rock Mech Mining Sci* 2009; 46: 699-707.
13. Rong G, Zhu HC and Zhou CB. Testing study on working mechanism of fully grouted bolts of thread steel and smooth steel. *Chinese J Rock Mech Eng*, 2004; 23: 469-475.

14. Moosavi M, Jafari A and Khosravi A. Bond of cement grouted reinforcing bars under constant radial pressure. *Cement Concrete Comp,* 200,5; 27: 103-109.
15. Martin LB, Tijani M and Hadj-Hassen F. A new analytical solution to the mechanical behaviour of fully grouted rockbolt subjected to pull-out tests. *Construction Building Materials*, 2011; 25: 749-755.
16. Martin LB, Tijani M, Hadj-Hassen F and Noiret A. Assesment of the bolt-grout interface behaviour of fully grouted rockbolt from laboratory experiments under axial loads. *Int J Rock Mech Mining Sci*, 2013; 63: 50-61
17. Martin LB, Hadj-Hassen F and Tijani M. A new experimental and analytical study of fully grouted rockbolts. *Proc. 45th US Rock Mechanics/Geomechanics Symposium*, 2011; ARMA11-242.
18. Hutchinson JW and Jensen HM. Models of fibre debinding and pullout in brittle composites with friction. *Mech Mater,* 1990; 9: 139-163.
19. Thouless MD. Frictional sliding and pull-out of a fibre. *Script Metall Mater*, 1992; 27: 1211-1214.
20. Tsai KH and Kim KS. The micromechanics of fibre pull-out. *J Mech Phys Solids*, 1996; 44: 1147-1177.
21. Beckert W and Lauke B. Finite element calculation of energy release rate for single-fibre pull-out test. *Comp Mater Sci,* 1995; 5: 1-11
22. Yang QS, Qin QH and Peng XR. Size effects in the fibre pullout test. *Comp Struct*, 2003; 61: 193-198.
23. Beckert W and Lauke B. Critical discussion of the single-fibre pull-out test: Does it measure adhesion? *Comp Sci Technol,* 1997; 57: 1689-1706.
24. Wang JS and Qin QH. Debonding criterion for the piezoelectric fibre pull-out test. *Philosophical Magazine Letters,* 2006; 86: 123-136.
25. ASTM E8M – 11 Standard Test Methods for Tension Testing of Metallic Materials.
26. ASTM D638-10 Standard Test Method for Tensile Properties of Plastics.
27. Suo Z and Hutchinson JW. Sandwich test specimen for measuring interface crack toughness. *Mater Sci Eng,* 1989; A107: 135-143.
28. Akisanya AR Fleck NA. Brittle fracture of adhesive joints. *Int J Fract,* 1992; 58: 93-114.
29. Banks-Sills L and Schwartz J. Fracture testing of Brazilian disk sandwich specimens. *Int J Fract,* 2002; 118: 191-209

30. Rice JR. Elastic fracture mechanics concepts for interfacial cracks. *J Appl Mech,* 1988; 55: 98-103.
31. Atkinson C, Smelser RE and Sanchez J. Combined mode fracture via Brazilian disk test. *Int J Fract,* 1982; 18: 279-291.

List of Tables

Figure Captions

Table 1:
Measured material parameters.
The manufacturer's quoted values, where available, are given in bracket.

	Steel bar	**Concrete**	**Resin grout**
Young's modulus [GPa]	203	31.0	7 (6.5)
Compressive strength [MPa]	-	64.3	(60)
Yield Strength [MPa]	600	-	-
Tensile Strength [MPa]	648	-	12
Poisson's ratio	0.30	0.20	0.32
Linear coefficient of thermal expansion K^{-1}	$\left(1.2\times10^{-5}\right)$	-	$\left(5.8\times10^{-5}\right)$

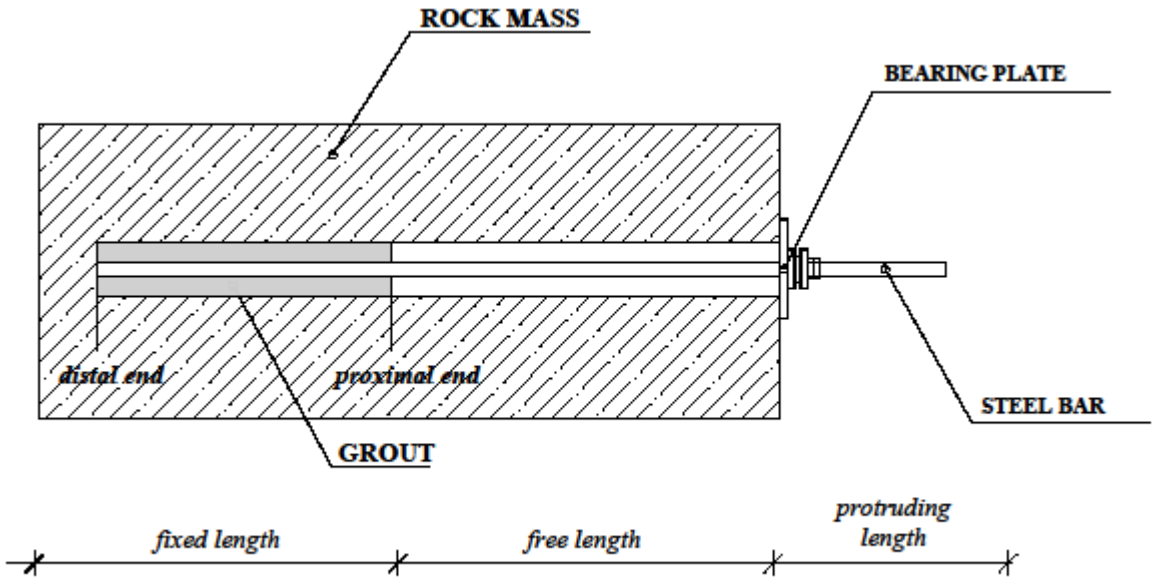
ROCK MASS
BEARING PLATE
distal end
proximal end
STEEL BAR
GROUT
fixed length
free length
protruding length

Figure 1

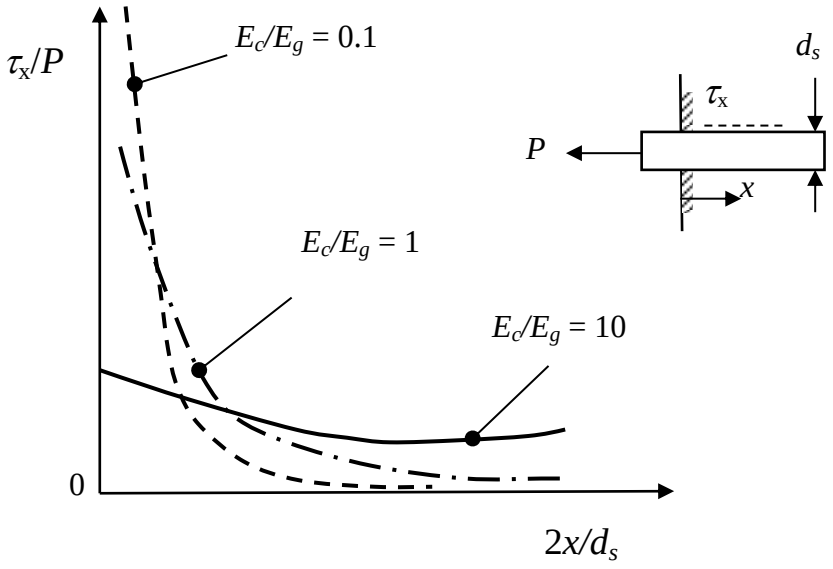

Figure 2

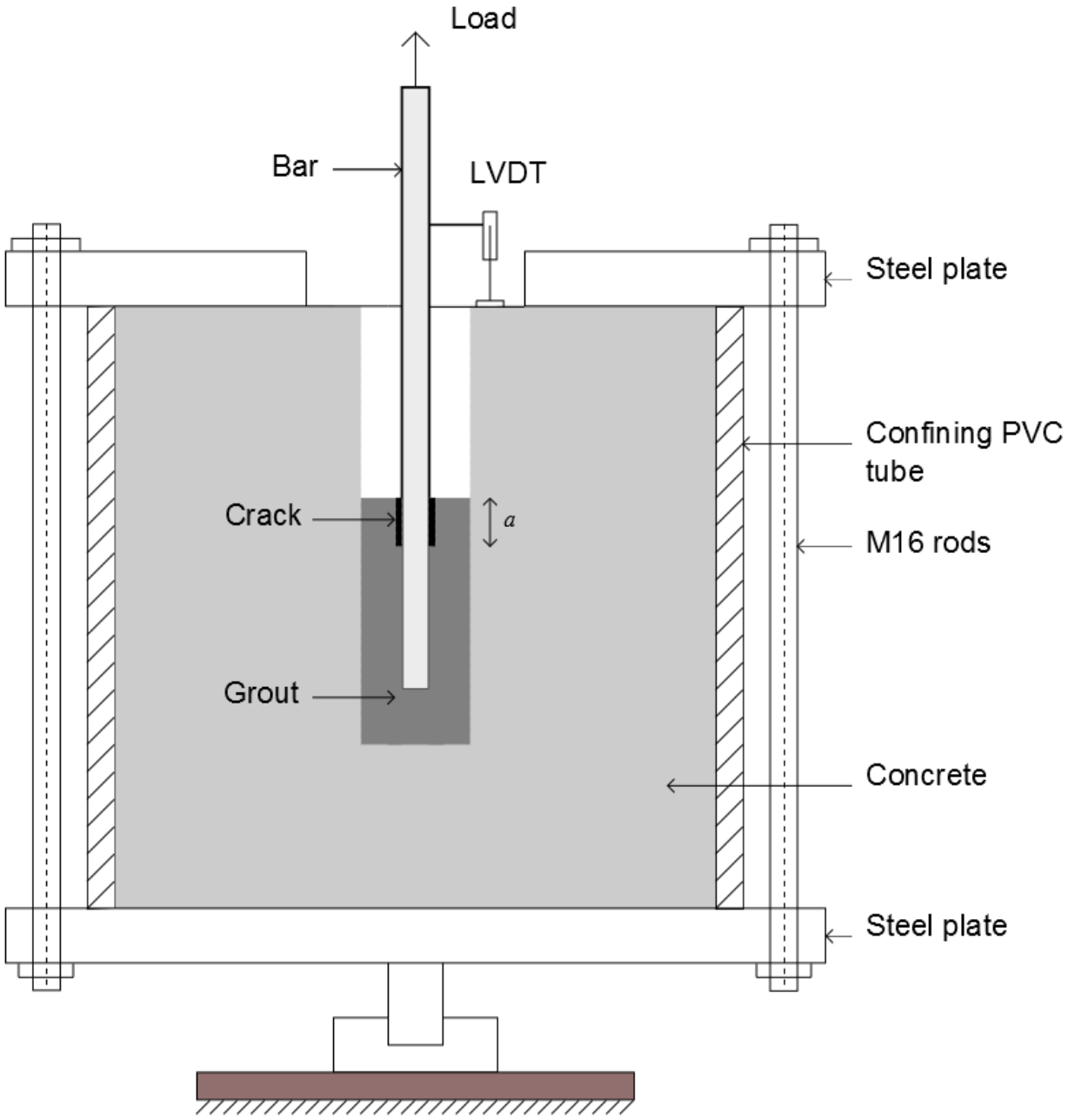
Load
Bar
LVDT
Steel plate
Confining PVC tube
Crack
a
M16 rods
Grout
Concrete
Steel plate

Figure 3a

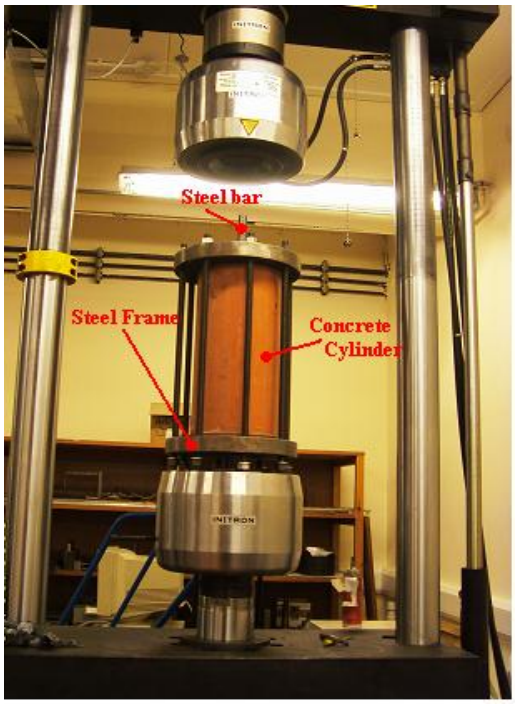

Figure 3b

Figure 4

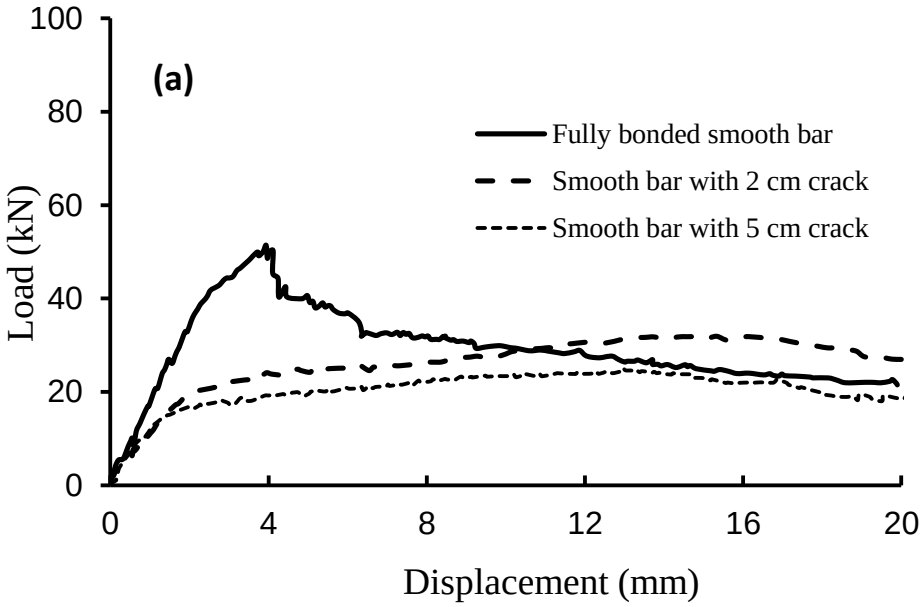
(a)
Fully bonded smooth bar
Smooth bar with 2 cm crack
Smooth bar with 5 cm crack
Load (kN)
Displacement (mm)
0
20
40
60
80
100
0
4
8
12
16
20

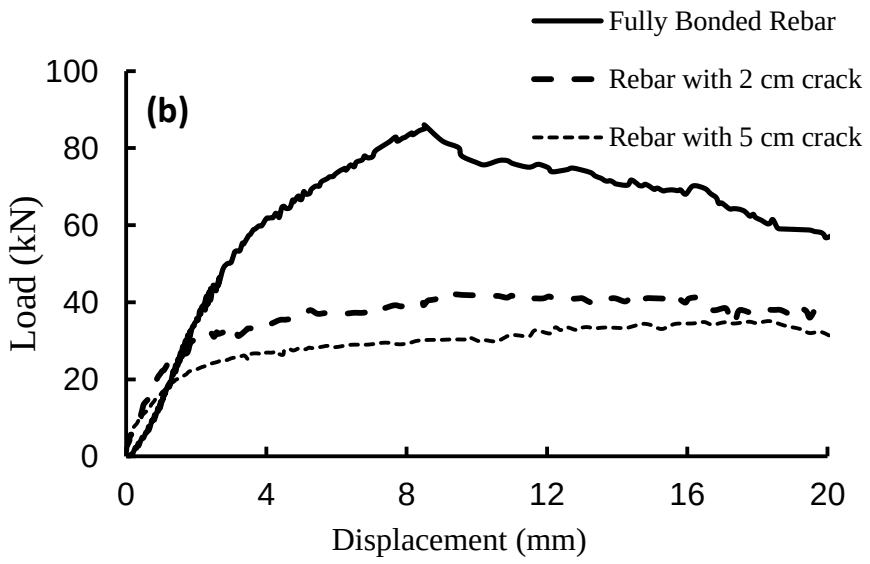
(b)
Fully Bonded Rebar
Rebar with 2 cm crack
Rebar with 5 cm crack
Load (kN)
Displacement (mm)
0
20
40
60
80
100
0
4
8
12
16
20

Figure 5

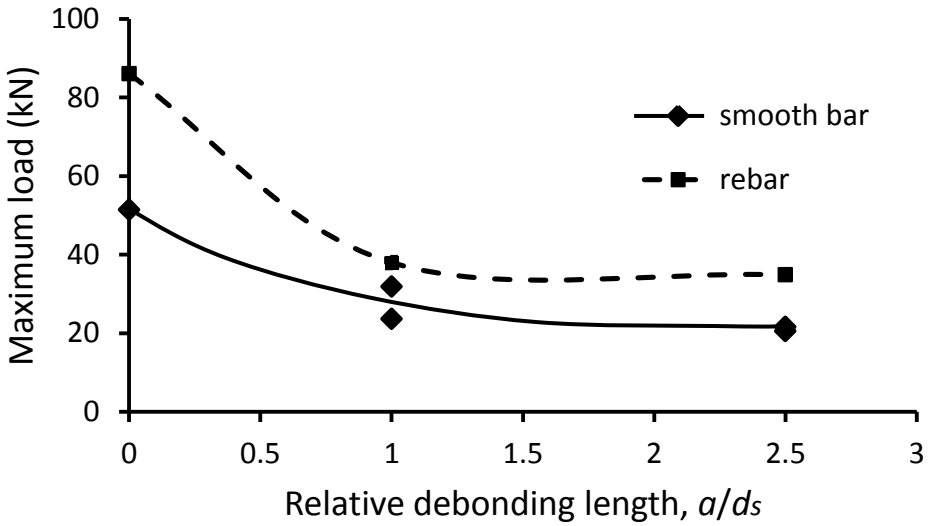
100
80
60
40
20
0
Maximum load (kN)
0
0.5
1
1.5
2
2.5
3
Relative debonding length, a/d_s
smooth bar
rebar

Figure 6

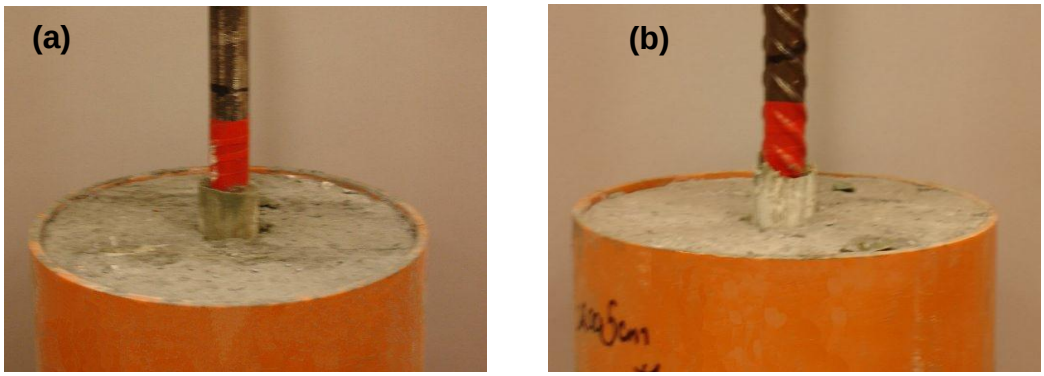

Figure 7

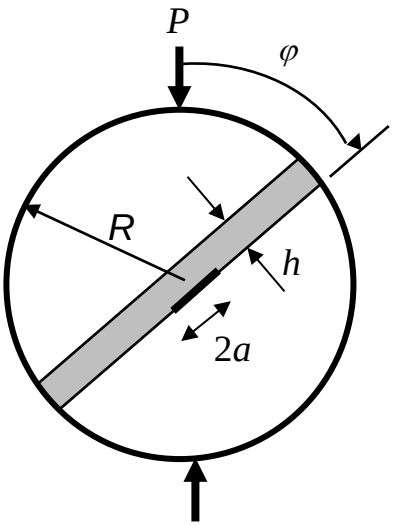

Figure 8

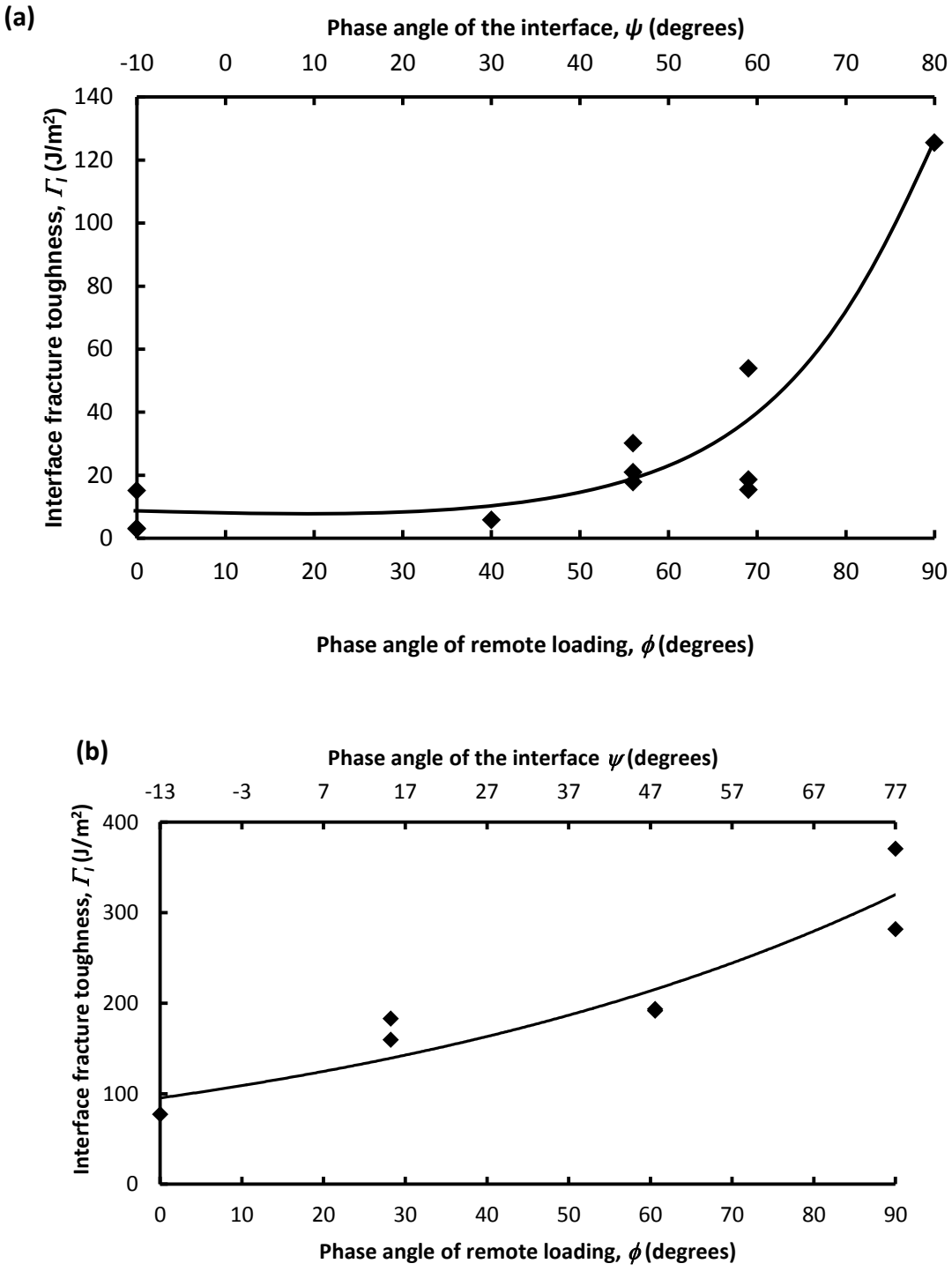
(a)
Phase angle of the interface, ψ (degrees)
-10 0 10 20 30 40 50 60 70 80
Interface fracture toughness, Γ_i (J/m²)
140 120 100 80 60 40 20 0
0 10 20 30 40 50 60 70 80 90
Phase angle of remote loading, ϕ (degrees)
(b)
Phase angle of the interface ψ (degrees)
-13 -3 7 17 27 37 47 57 67 77
Interface fracture toughness, Γ_i (J/m²)
400 300 200 100 0
0 10 20 30 40 50 60 70 80 90
Phase angle of remote loading, ϕ (degrees)

Figure 9